

See discussions, stats, and author profiles for this publication at: <https://www.researchgate.net/publication/273169659>

Curved Silicon Micromirror for Linear Displacement-to-Angle Conversion With Uniform Spot Size

Article in IEEE Journal of Selected Topics in Quantum Electronics · July 2015

DOI: 10.1109/JSTQE.2014.2375493

CITATIONS
23

READS
983

4 authors:



Yasser Mohammed Sabry

Ain Shams University

172 PUBLICATIONS 1,104 CITATIONS

[SEE PROFILE](#)



Diaa Khalil

Ain Shams University

333 PUBLICATIONS 2,166 CITATIONS

[SEE PROFILE](#)



Bassam Saadany

si-ware systems

47 PUBLICATIONS 911 CITATIONS

[SEE PROFILE](#)



T. Bourouina

Université Paris-Est, ESIEE Paris

301 PUBLICATIONS 4,852 CITATIONS

[SEE PROFILE](#)

Some of the authors of this publication are also working on these related projects:



Microwave photonics [View project](#)



Infrared meta-materials for thermal radiation sensing, conversion and management [View project](#)

Curved Silicon Micromirror for Linear Displacement-to-Angle Conversion With Uniform Spot Size

Yasser M. Sabry, *Member, IEEE*, Diaa Khalil, *Senior Member, IEEE*, Bassam Saadany, and Tarik Bourouina, *Senior Member, IEEE*

Abstract—This paper reports a novel class of deeply etched curved micromirrors enabling linear conversion between the reflection angle of incident light beam and displacement of the beam axis with respect to the curved mirror principal axis. Moreover, the mirror provides phase-transformation of the light beam independent of the inclination angle of the incident light on the mirror surface. The micromirrors are fabricated on SOI substrate by deep reactive ion etching technology. The profile of the curved surface is optimized and controlled precisely, thanks to the photolithographic process. High optical throughput micromirrors exhibiting submillimeter focal lengths are fabricated with 200- μm etching depth and with a sidewall angle deviation from perfect verticality, which is smaller than 0.1°. Optical measurements at wavelengths of 675 and 1550 nm show transformation of the optical beam with high optical spot size stability during a beam steering process with less than $\pm 5\%$ dependence on the inclination/reflection angle over a scanning angle range of 120°. The presented micromirror has applications in MEMS scanners, displacement/rotation sensing, and optical imaging.

Index Terms—Curved micro-optics, displacement sensor, DRIE, MEMS optical bench technology, optical scanner.

I. INTRODUCTION

SILICON micromachined curved mirrors were reported in literature for a wide range of applications [1]–[11]. These mirrors can be classified according to the orientation of their principal axis. Curved mirrors with in-plane principal axis are found in micro-optical benches etched using deep reactive ion etching (DRIE) technology on silicon or silicon-on-insulator (SOI) substrates. Having their axis parallel to the substrate enables the integration of this type of mirrors with other micro-optical and micro-electro-mechanical components on chip. Deeply-etched micromirrors with circular, parabolic

or elliptical cross sections were reported for the purpose of making variable optical attenuation [2], [3], increasing the coupling efficiency of tunable lasers [4] and improving the quality factor of optical cavities [5]. The reported micromirrors have conventional surface profiles and are used to treat free-space propagating optical Gaussian beams (GBs) only for a given inclination angle. Consequently, any variation in the inclination angle will lead to variation in the properties of the reflected beam. Recently, a micro-optical bench comprising acylindrical micromirror was introduced [6], where the profile of the acylindrical micromirror was generated in a specific way coupled to the motion of a MEMS actuator with a one degree-of-freedom. The system was optimized to minimize the above mentioned variation but not eliminating it all together, even theoretically. The etching depth of optical components using DRIE on SOI substrates is usually limited to 100 μm . Deeper etch of the optical components can be achieved using alkaline solutions [12], where the wet anisotropic etching yields very high surface quality and vertical surface close to ideal but on the expense of: (i) restricting only to flat optical surfaces arrangement and (ii) prohibiting the deep etching of in-plane curved surfaces. The other category of curved micromirrors has principal axis oriented out-of-plane with respect to the substrate. Silicon curved micromirrors fabricated on wafer top surface were reported using isotropic chemical etching for the sake of optical detection of single atom [9], using selective polishing method on the top of MEMS tunable VCSEL [10] and using ion beam irradiation and electrochemical etching for atomic studies as well as optical interconnects [11]. However, having the principal axis of the class of mirror being oriented out-of-plane renders the mirror incompatible with monolithically-integrated silicon micro-optical bench systems where the light is propagating in-plane with respect to the substrate.

Consider the off-axis incidence of a beam on a curved mirror with an incidence angle θ_{inc} as shown in Fig. 1, in which the displacement between the axis of the beam and the micromirror leads to a change in the reflection angle. In fact, conversion of mirror's translational displacement to angular deflection of the light beam is the main task carried out by lens-based or curved mirror-based optical scanners [6], [13]–[16]. The use of curved micromirrors has the advantages of achieving wide-angle scanning and avoiding chromatic aberration with respect to micro lenses. Another important requirement in such scanners is the need to keep the uniformity of the optical beam spot dimensions while scanning and to correct the nonlinearity of the scanning

Manuscript received September 12, 2014; revised November 6, 2014; accepted November 21, 2014. This work was supported in part by the ITAC funding program of the Information Technology Industry Development Agency in Egypt.

Y. M. Sabry was with Université Paris-Est, ESIEE Paris, Noisy-Le-Grand F-93162, France. He is now with the Faculty of Engineering, Ain Shams University, Cairo 11517, Egypt (e-mail: ysabry@ieee.org).

D. Khalil is with Faculty of Engineering, Ain Shams University, Cairo 11517, Egypt (e-mail: diaa.khalil@ieee.org).

B. Saadany is with the Optical MEMS Technology Division, Si-Ware Systems, Cairo 80309, Egypt (e-mail: bassam.saadany@si-ware.com).

T. Bourouina is with Université Paris-Est, ESIEE Paris, Noisy-Le-Grand F-93162, France (e-mail: tarik.bourouina@esiee.fr).

Color versions of one or more of the figures in this paper are available online at <http://ieeexplore.ieee.org>.

Digital Object Identifier 10.1109/JSTQE.2014.2375493

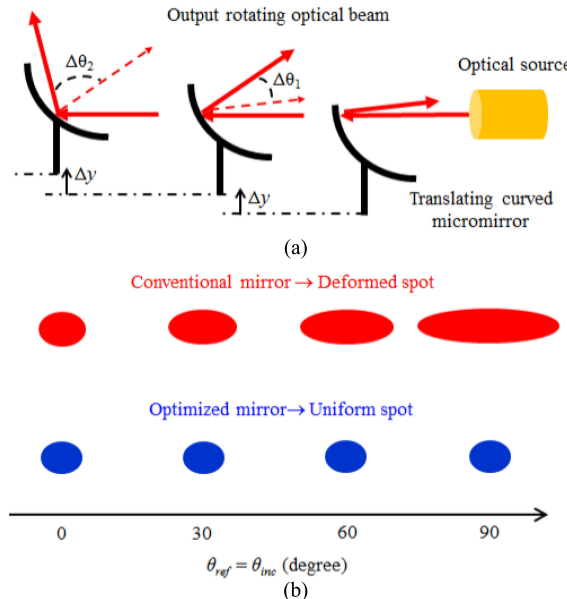


Fig. 1. (a) Illustration for the basic idea of causing angular deflection for the optical beam by translating a curved micromirror by a MEMS actuator not shown in the drawing. (b) Comparison between the performance of conventional and optimized micromirror profiles in terms of the reflected spot size versus the incidence angle. The use of curved micromirror in scanning has the advantages of achieving control of spot uniformity, but also wide angle scanning and overcoming achromatic aberration, when compared with the use of lenses.

system, in which the displacement is usually proportional to the tangent of the scan angle, rather than to the angle directly [17], [18]. In fact the linear conversions requires that $\Delta\theta_1 = \Delta\theta_2$ in Fig. 1(a) while uniform spot scanning versus deformed spot is shown in Fig. 1(b). These requirements are not only needed in microscanning for display and imaging applications but also in laser micro-processing of material such as drilling [19], dicing, structuring and engraving applications [20]. The conversion of displacement to angular deflection is needed also in optical bio-analytical applications such as wavelength-to-angle mapping [21] and scanning flow cytometer for beads analysis [22]. In a previous report [6], we started addressing this important issue but the requirement of linearity has not been satisfied, while the spot uniformity was not fully attained even theoretically. As demonstrated in this paper, achieving such requirements is possible by simultaneously optimizing the micromirror's curvature profile and its displacement trajectory.

In order to build microsystems in the optical bench fashion, a wide library of deeply etched micro-optical components has been introduced including flat and cylindrical metalized micromirrors, flat and cylindrical distributed Bragg reflectors, thin as well as half-plane silicon beam splitters, diffraction gratings including blazed-type and lamellar-type grating, antireflective-coated surfaces, corner cube reflectors and acylindrical micromirrors [23]. Indeed, a broad range of miniaturized optical devices has been implemented combining one or more of the micro-optical component together with MEMS actuators. More specifically, variable optical attenuators [24], optical accelerometer [25], optical tunable filters [26]–[28], diffraction

grating-based and two/multiple beam-based interferometers [28]–[30], optical cavities [31], external cavity tunable lasers [32], Fourier-transform spectrometers [33]–[35] and more recently integrated wide-angle microscanners [6], [36] and swept laser sources [37]. However, a curved micromirror with an optimized profile fulfilling the needs mentioned previously was not reported.

The objective of this work is to introduce a curved micromirror that can maintain the spot size uniformity versus scanning and in the same time, can provide linear relationship between the displacement of an optical beam and its inclination angle, in a micro-optical bench system. The rest of this article is organized as follows. Theoretical results based on GB transformation by curved elements are presented in Section II. The design and analysis of the introduced class of curved micromirrors satisfying the needs mentioned above are given in Section III. Optical simulation results for the presented as well as the conventional cylindrically curved surfaces—based on the simplified Gaussian-optics approach—are discussed in Section IV. The simulation is complemented by Fourier-optics approach in order to examine the quality of the optical spot produced by the curved micromirrors. The fabrication results of the micromirror on SOI substrate using DRIE are given in Section V emphasizing on the quality of the produced optical surface. The optical measurement results are presented in Section VI showing the superiority of the presented micromirror in comparison with a cylindrical surface used as reference. Finally, the work is concluded in Section VII.

II. THEORETICAL BACKGROUND

In Gaussian-optics treatment of optical systems, an incident GB remains Gaussian after reflection or refraction from the optical element. Dealing with off-axis reflection upon the surface of a curved mirror, this approach is based on the assumptions that the beam diameter is small relative to the radius of curvature of the off-axis curved mirror, where a symmetric quadratic expansion for the curved surface is assumed around the incidence point. Consider the off-axis incidence of a GB on a curved mirror having a radius of curvature R with an incidence angle θ_{inc} as shown in Fig. 2(a). The off-axis incidence can be considered as a rotation of the mirror around the x -axis (outward direction of the tangential plane). For a spherical curved reflector, the projection will be elliptical on the x - y plane with the minor axis along the y -axis. In this case, the y - z plane is called the tangential plane while the x - z plane is the sagittal plane. Now the elliptical projection of the mirror is still having mirror symmetry around x - and y -directions such that each direction can be treated independently. The mirror becomes an astigmatic component with different focal lengths f_t and f_s in the tangential and sagittal planes. In our case we will be dealing with a curved profile in the tangential plane and flat profile in the sagittal plane defined by photolithography and DRIE. The mirror, therefore, has infinite focal length in the sagittal plane while the tangential plane focal length is given by [38]:

$$f_t = -0.5R \cos \theta_{inc}. \quad (1)$$

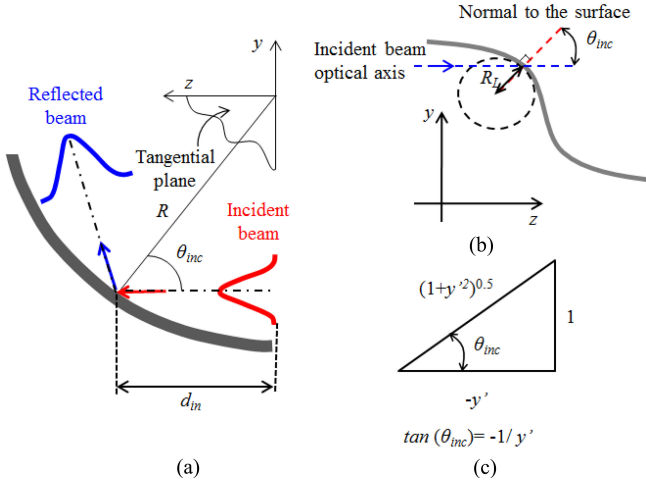


Fig. 2. (a) Off-axis incidence of a Gaussian beam on a curved mirror with an inclination angle θ_{inc} where the mirror radius of curvature is R . (b) Illustration for the local radius of curvature (R_L) at the point of incidence of the optical beam on the curved surface. (c) Trigonometric triangle showing the relation between the derivative of the surface profile and the incidence angle.

Based on the Gaussian-optics approach, the reflected GB spot radius w_{out} in the tangential plane is related to the incident GB counterpart by (2):

$$w_{out} = \frac{w_{in}}{\sqrt{(1 - f^{-1}d_{in})^2 + f^{-2}z_o^2}} \quad (2)$$

where w_{in} is the spot radius of the incident GB, d_{in} is the distance between the location of the incident GB waist and the point of incidence on the curved mirror and z_o is the Rayleigh range of the incident GB given by $\pi w_{in}^2/\lambda$. (1) and (2) will be used in the rest of this article to study the effect of changing the incidence angle on the curved mirror on the output spot size uniformity in the case of the conventional as well as the presented curved mirror.

The last important concept to highlight in the theoretical background section before going to the next section is the local radius of curvature (R_L) on the curved mirror surface. The local radius of curvature of a curved surface at a point is defined by the distance measured between the point and the center of curvature of the surface at that point (see Fig. 2(b)). An imaginary circle can be drawn around the center of curvature while being tangential to the surface at the desired point. The local radius of curvature is equal to the radius of curvature of this imaginary circle. Mathematically, it is defined by [39]:

$$R_L = \frac{(1 + y'^2)^{3/2}}{y''} \quad (3)$$

where y' is the first derivative of y with respect to z and y'' is the second derivative of y with respect to z . The z - y coordinate system is oriented such that the incident beam axis is parallel with respect to the z -axis. The local radius of curvature R_L can be either positive or negative depending on whether the curvature is looked at from the convex or the concave face of the profile. In this orientation, the tangent of the incidence

angle θ_{inc} of the incident beam is given by the negative of the reciprocal of the slope of the profile at the incidence point. The cosine of the incidence angle θ_{inc} , which is of interest to define the focal length of the curved surface, can then be derived with the aid of the trigonometry triangle shown in Fig. 2(c) as:

$$\cos(\theta_{inc}) = \frac{-y'}{(1 + y'^2)^{0.5}}. \quad (4)$$

III. CURVED MICROMIRROR DESIGN

Curved micromirrors can be used to transform the transverse displacement of optical beams—or the displacement of the mirror surface with respect to optical beam—to angular deflection. For the conventional cylindrical surfaces, the profile is given by:

$$y = y_o + \sqrt{R_C^2 - (z - z_o)} \quad (5)$$

where R_C is the constant radius of curvature of the cylindrical surface, (z_o, y_o) are the coordinates of the center of curvature of the surface. The displacement y and the angular deflection θ_{inc} are related by:

$$\theta_{inc} = \cos^{-1} \left[\frac{\sqrt{R_C^2 - (y - y_o)^2}}{R_C} \right]. \quad (6)$$

It is clear that the relation in (6) is highly non-linear highlighting the need for a micro curved surface providing a linearized relation. In fact the root cause of the non-linearity in the cylindrical micromirrors is that local focal length of the mirror—defined by the multiplication of one half the local radius of curvature and the cosine of the incidence angle—is not constant across the profile of the curved micromirror. In addition to causing non-linearity, the variation of the focal length across the mirror surface renders the spot of the reflected beam being deformed during scanning. It then appears that keeping the focal length of the curved surface constant and independent of the incidence angle is fulfilled by the introduction of a new class of acylindrical surface profile satisfying the following condition:

$$-0.5R_L(\theta_{inc})\cos(\theta_{inc}) = \text{constant} = f_o \quad (7)$$

where R_L is a function of the inclination angle, leading to an acylindrical shape for the mirror, and f_o is the desired focal length of the curved surface. Substituting for the radius of curvature of the surface by (3) and the cosine of the inclination angle by (4), (7) can be rewritten as a second order non-linear differential equation:

$$2f_o y'' - y'^3 - y' = 0. \quad (8)$$

The analytical solution of (8) was found and arranged in the expression of (9):

$$y = y_v - 2f_o \tan^{-1} \left(\exp \left[\frac{-z_v}{2f_o} \right] \sqrt{\exp \left[\frac{z}{f_o} \right] - \exp \left[\frac{z_v}{f_o} \right]} \right) \quad (9)$$

where z_v, y_v are the curved surface vertex coordinates. Now to find the relationship between the displacement y and the incidence angle (or the reflection angle) θ_{inc} , we have to find the

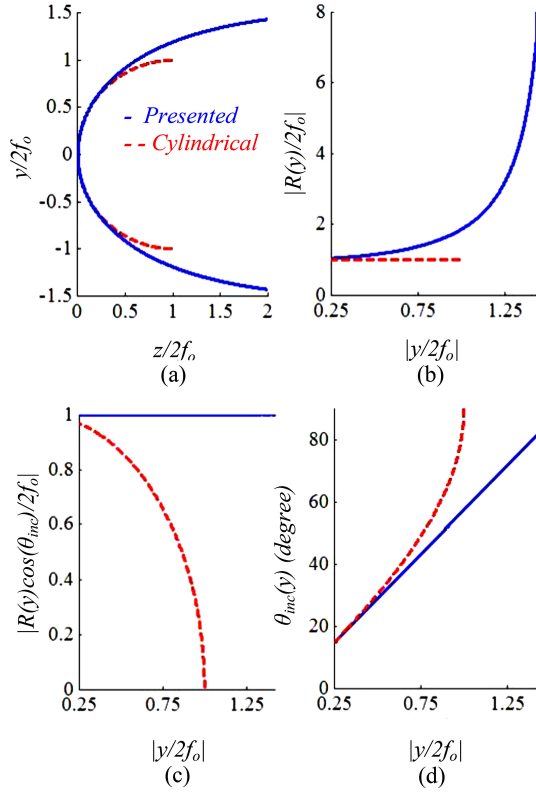


Fig. 3. Comparisons between the profiles of the presented mirror surface and the conventional cylindrical one where f_o is the focal length and z/y are the Cartesian coordinate system. (a) Cross sectional mirror profile. (b) Local radius of curvature. (c) Multiplication of the radius of curvature by the cosine of the inclination angle. (d) The inclination angle versus the distance between the axis of the beam and the axis of the mirror.

derivative of (9) with respect to z . Given that $d/dx[\tan^{-1}(x)] = 1/(1+x^2)$, one can find that:

$$\theta_{inc} = \frac{y}{2f_o}. \quad (10)$$

A comparison between the presented surface and the conventional cylindrical profile is given in Fig. 3 where $(x_v, y_v) = (0, 0)$ for simplicity. The local radius of curvature of the surface has the following properties. It has its smallest value at the vertex of the surface and increases monotonically away from the vertex. It increases gradually with $|y|$ away from the vertex to about $|y| \sim 2f_o$ then it increases rapidly. The cosine of the inclination angle decreases gradually with $|y|$ such that multiplying the radius of curvature by the cosine of the inclination angle remains constant at any portion or point of the surface and is equal to $2f_o$. This perfectly constant behavior is a unique feature of the presented profile. Having the focal length of the curved surface constant with inclination maintains the dimensions of the spot size (of the optical beam reflected by the mirror) stable versus inclination.

In fact this stability requires also maintaining constant distance between the location of the incident GB waist and the point of incidence on the curved mirror. This can be achieved by displacing the mirror on curved trajectory using two degree of freedom actuator with proper electronic control. The curved

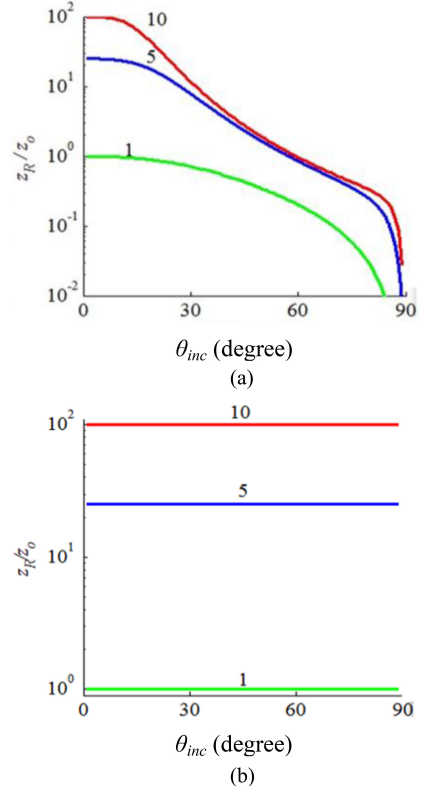


Fig. 4. Gaussian-optics simulation results for the ratio between the Rayleigh range of the reflected and incident beams versus the incidence (or reflection) angle. The results in the case of the conventional cylindrical surface are given in (a) while the case of the presented surface is given in (b). The study is carried out for f_o/z_o ratios of 1, 5 and 10. Uniform output beam parameters can be obtained using the presented surface.

trajectory profile is exactly the same as the mirror profile described by (10). The second unique property of the presented curved mirror is that the inclination angle, and thus the reflection angle, varies linearly with the vertical displacement of the incident beam with respect to the horizontal axis. Indeed, this linear relation between the inclination angle and the displacement is ideal for the optical scanning and sensing applications.

IV. OPTICAL SIMULATION RESULTS

In this section we carry out a simulation study for the reflected GB Rayleigh range and spot quality for the presented curved surface and compare it to the conventional cylindrical surface. The study is carried out versus the angle of incidence at different ratios between the focal length of the curved surface and the Rayleigh range of the incident beam. Based on the transfer matrix approach, the ratio between the Rayleigh range of the reflected beam (z_R) and the Rayleigh range of the incident beam (z_o) was calculated and plotted versus the incidence angle for f_o/z_o values of 10, 5 and 1. The results are depicted in Fig. 4(a) and (b) for the case of a conventional cylindrical surface and the presented surface, respectively. In the cylindrical surface case, the ratio varies significantly with the incidence angle where the variation amplifies with the ratio f_o/z_o . For example, a 10% reduction in z_R/z_o is found at 10, 13 and 25° for f_o/z_o of 10,

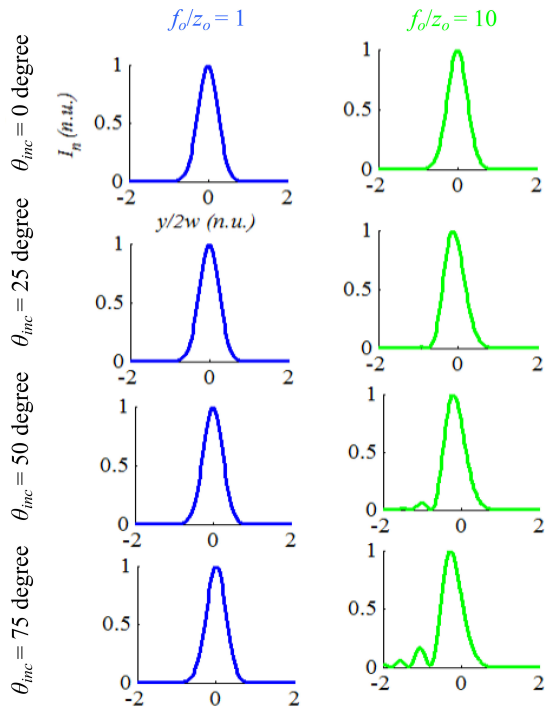


Fig. 5. Beam intensity profile reflected on the presented curved surface. The profile was obtained using Fourier-optics simulation approach. The profile is examined for f_o/z_o ratios of 10 and 1 and for incidence angles of 0° , 25° , 50° and 75° .

5 and 1 respectively. The significant roll-off in the Rayleigh range of the output beam is a critical drawback in the scanning performance based on a cylindrical reflector. On the other hand, uniform reflected beam Rayleigh range is obtained using the presented surface without any degradation versus the incidence angle and up to 90° ; corresponding to 180° optical deflection angle.

The Gaussian-optics approach is sufficient to describe accurately the reflected beam as long as the radius of curvature of the mirror is much larger than the spot radius of the incident GB. In this work we are interested in curved micromirrors, in which this assumption may not be valid. For this reason, a diffractive Fourier-optics approach was adopted and the curved micromirror surface is treated as a phase transformation element without approximating the curved surface to a parabolic profile. The incident GB is regarded as a superposition of plane waves which are the natural modes of the propagation in free-space. The curved phase front of the GB can be synthesized from a large number of plane wave phase fronts oriented in different directions in space [40].

The Fourier-optics simulation wavelength was set to $\lambda = 1550$ nm and the mirror focal length was set to $f_o = 200 \mu\text{m}$. The GB waist size was varied in order to have f_o/z_o ratios of 10 and 1. Indeed, using a polynomial representation for fitting the surface in (9) results in non-accurate results because of the radius of curvature of the surface described by the polynomial being not matching that of the surface. Therefore, the exact equation has to be used. The intensity profile was obtained for incidence angles of 0° , 25° , 50° and 75° as shown in Fig. 5. The

profiles are distortion-free even for the case of 75° incidence angle when $f_o/z_o = 1$. For $f_o/z_o = 10$, the output profile peak shifts to the left with increment in the incidence angle and side lobes appears clearly for 75° incidence angle. The small artifacts at large f_o/z_o ratios up to 10 seem to be still acceptable for many applications.

V. MICROMIRROR FABRICATION

The profile of the curved surface has unique features in terms of how its radius of curvature and the slope of the surface at any point on it—with respect to its axis—change across the surface. The surface cannot be described with a rotationally symmetric (or asymmetric) polynomial without changing the optical properties of GB transformation using the surface. This is because the surface profile contains information not only about the vertical coordinates versus the horizontal coordinates but also information about the slope and the radius of curvature of the profile for each small portion of the curve. Such information is hard to keep accurate even with high order polynomial due to the small oscillation of the polynomial around the exact values. Moreover, the presented class of curved mirrors was designed targeting the monolithic integration into micro-optical benches. Therefore, the curved micromirror surface was fabricated using DRIE on SOI wafer. The surface profile could be also accurately defined by feeding the surface equation to a layout editor, mask generation and photolithography.

On the other hand, from an optical system point of view following a light source, the optical throughput is the area of the entrance aperture times the solid angle the source subtends as seen from the aperture [41]. The optical throughput is a quantitative measurement of how much light energy gets through an optical instrument. As a consequence of the limited micromirrors size in micro-optical benches, deeply-etched micro-optical benches usually have low optical throughput, insufficient to serve an adequate signal to noise ratio in miniaturized sensors and instruments. In fact, obtaining optical surface quality over depth that is larger than $100 \mu\text{m}$ using DRIE is challenging. This is especially true for micro-optical designs embedding relatively wide etching areas around the optical surfaces. An intensive review of the different DRIE processes and their limits can be found in ref. [42]. Usually alkaline etching on crystalline planes is incorporated to achieve large depth and good surface quality [43]. In our case, we had to avoid the use of alkaline etching because it is harmful for designed curvature of curved micromirrors and results in segmented surface, instead.

A typical DRIE profile is shown in Fig. 6(a), where the height is h , the sidewall angle is β and scalloping depth due to the DRIE Bosch process is d . An etching depth in the order of $200\text{--}300 \mu\text{m}$ is required for relatively large optical throughput. The scalloping depth is required to be less than 75 nm that is about $\lambda / 20$ where λ is the wavelength of light in the near infrared spectrum (around 1550 nm) [44]. The verticality of the sidewall angle is important to keep the parallelism between the optical beam axis and the substrate plane. This is to avoid optical beam clipping and to allow the integration of many micro-optical components within the optical bench, without sacrificing the latter's performance.

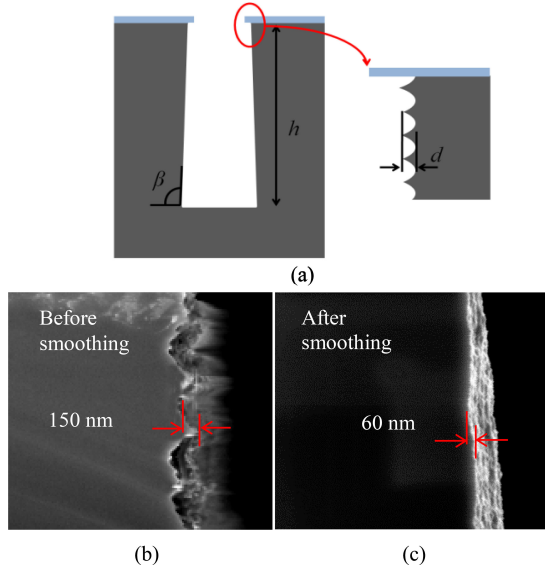


Fig. 6. (a) Schematic illustration of etched profile with height h , sidewall angle β and scalloping depth d . (b) DRIE scallops before smoothing. (c) DRIE scallops after smoothing. The scalloping depth was reduced from about 150 nm to about 60 nm.

In fact, with optimization of the DRIE process on silicon wafers we were able to reach a verticality that is better than $90 \pm 0.1^\circ$ over an etching depth that is slightly larger than 300 μm on silicon substrates.

The use of an SOI wafer enables the release of the curved mirror and its attachment to a movable comb-drive MEMS actuator. The device layer height of the SOI wafer is chosen to 200 μm in order to have sufficient optical throughput for the micromirror while keeping practical comb-drive dimensions and reasonable requirements on the electrical voltage to drive the comb-drive. On the SOI substrate, the curved micromirror was obtained also with a sidewall angle whose deviation from the perfect verticality is smaller than 0.1 degree. Followed by an oxidation and oxide etching smoothing step to reduce the scallops resulting from the optimized DRIE process, peak-to-peak surface roughness in the order of 60 nm was obtained, as shown by the SEM images in Fig. 6(b) and (c), forming a high-quality optical surface. The reflectivity of the micromirror after aluminum coating of the surface was measured and found to be larger than 90%.

SEM images for the fabricated curved micromirror and overall device are shown in Fig. 7. An electrostatic comb-drive actuator is used to displace the mirror according to the applied voltage. The comb-drive is balanced and works in push-pull operation in order to produce large displacement and a double-folded spring (see Fig. 7(a)) is used to avoid the mechanical non-linearity [45], [46]. The comb-drive motion achieves a peak-to-peak displacement of 400 μm , around the rest position [6]. The curved mirror is attached to the comb-drive actuator using a relatively rigid but released arm, as shown in Fig. 7(b) where the connection point is not shown in the figure. A zoom-in on the curved micromirror is given in Fig. 7(c). Curved micromirrors with focal lengths of 100, 200 and 400 μm were fabricated and their measurements results will be shown in next section. The micromirrors were

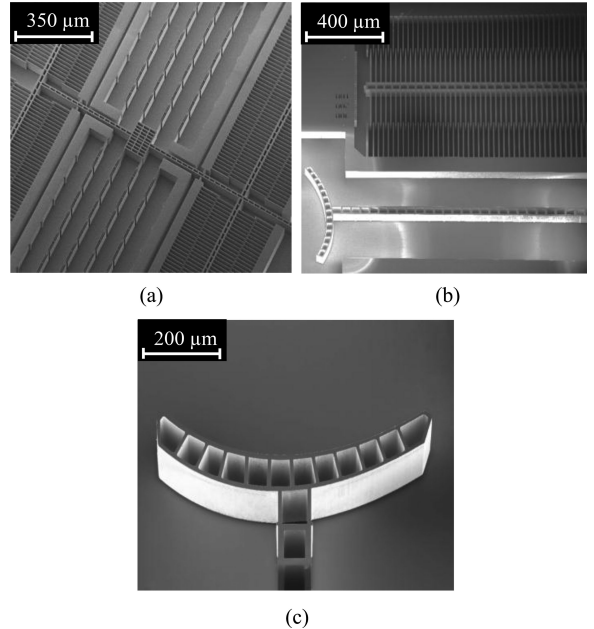


Fig. 7. SEM images of the fabricated comb-drive and curved micromirror with the presented profile. (a) The comb-drive actuator and its folded spring. (b) The mirror arm attached to the comb-drive and the metallized area around the mirror. (c) Close view of the curved mirror.

metallized using aluminum through shadow mask technique to improve their optical reflectivity. It is important to mention that achieving the full capabilities of the mirror for maintaining uniform spot size in scanning requires two degree of freedom translational motion. For the purpose of demonstrating a proof of concept of this capability, an external displacement has been used to complement the one degree of freedom motion of the comb-drive shown in Fig. 7(a).

VI. EXPERIMENTAL OPTICAL MEASUREMENTS

Optical measurements were carried out in order to characterize the scanned beam spot size and intensity profile versus different inclination angles. A 4/125 OZ Optics optical fiber was fed from a 675 nm laser source to generate a GB in the visible spectrum. The optical fiber was inserted on the substrate with its axis aligned to the principal axis of the curved micromirror. The fiber position was adjusted to have collimated reflected beam. Other positions are also possible, for example for having focused beam. The inclination angle between the optical beam and the surface of the micromirror could be controlled by varying the displacement between the optical fiber axis and the principal axis of the curved micromirror while keeping fixed distance between the optical fiber cleaved face and the micromirror surface. The reflected beam spot size and intensity profile were captured using DataRay Inc. BeamScopeTM-P8 scanning slit beam profiling system. A comparison between the resulting beam spot radius using the presented micromirror and the conventional cylindrical one is shown in Fig. 8, where the variations in the beam spot radius are minimal for the case of the presented micromirror. The experimental results agree well with our theoretical predictions.

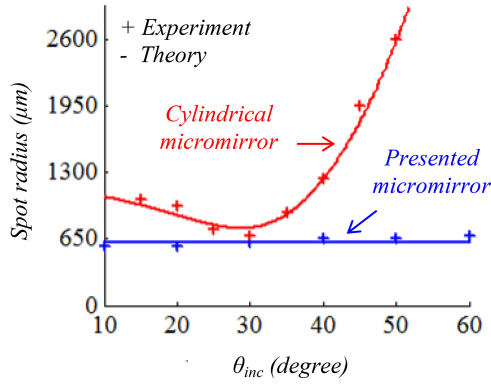


Fig. 8. Reflected beam size versus inclination angle θ_{inc} at $\lambda = 675$ nm using the presented micromirror and the conventional cylindrical profile.

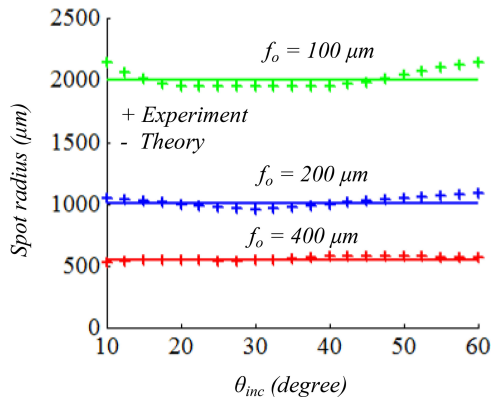


Fig. 9. Reflected beam size versus inclination angle θ_{inc} using the presented micromirror at $\lambda = 1550$ nm for different focal lengths.

Optical measurements were also carried out using a standard single-mode fiber fed from a laser source operating at 1550 nm. The experiment was conducted for micromirror focal length f_o of 100, 200 and 400 μm and the results are shown in Fig. 9. The optical beam spot variation is less than $\pm 5\%$ up to 60° inclination angles. Again there is a good agreement between the experimental results and the theoretical predictions at 1550 nm wavelength, thanks to the achromatic behavior of the mirror. Indeed, the near infrared operation of a wide-angle optical scanner based on the presented micromirror has direct application in biomedical imaging, for example optical coherence tomography. On the other hand, implementing a MEMS scanner working in the visible spectrum of light using the presented curved mirror has potential application in display and microscopic imaging. The achievable scanning angle is 120° as twice as the inclination angle.

The measured normalized intensity profile of the beam along the transverse direction is shown in Fig. 10 for inclination angles of 10° and 50°. The profiles show very good agreement with the theoretical Gaussian intensity profile highlighting the high optical quality of the presented curved micromirrors. Gaussian fitting of the data results in a root mean square error that is less than 3%. The reflected beam spot is of elliptical type because the micromirror is flat in the out-of-plane direction with respect the

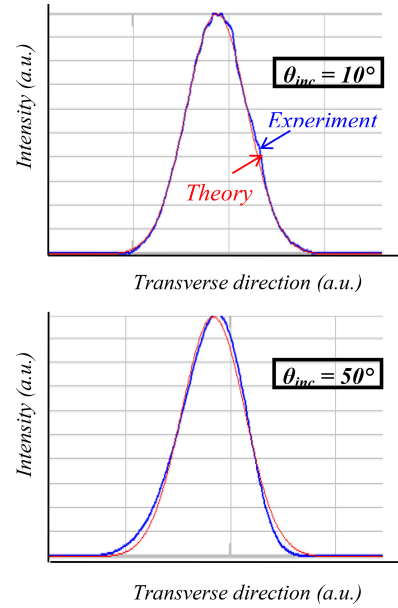


Fig. 10. Reflected beam profiles for given inclinations (of 10 and 50 degrees) using the presented micromirror at $\lambda = 1550$ nm.

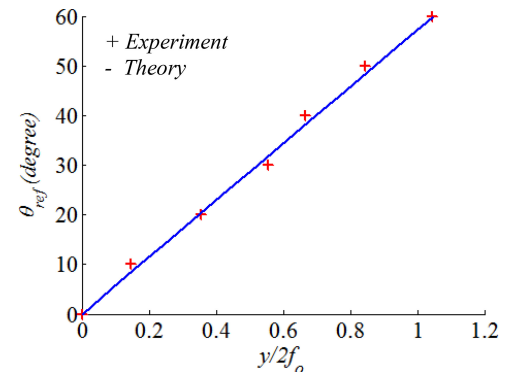


Fig. 11. Relation between the reflected beam angle and the vertical displacement of the incident beam with respect to the horizontal axis of the micromirror.

silicon substrate. In fact, achieving curved profile in the out-of-plane direction is possible based on plasma etching, as recently reported in refs. [7], [8]. Maintaining the spot uniformity in both in-plane and out-of-plane directions may be possible by the accurate control of the three-dimensional profile of the mirror as suggested in ref. [47].

The linear relation between the incident beam angle, or reflected angle, and the displacement was verified as shown in Fig. 11. The measurement was carried out on the micromirror with the largest focal length to reduce the effect of the micro positioner calibration errors. The displacement is normalized to twice the focal length, so that comparing with the linear theoretical relation in (10) is possible.

VII. CONCLUSION

A curved acylindrical micromirror with optimized profile was presented, studied using theoretical analytical modeling

and measured experimentally in an MEMS optical scanner implementation. Besides the large quasi-static scanning angles of more than 120°, which are accessible free of chromatic aberration, the unique features of the presented mirror include a linear relation of displacement versus angle and almost no distortion of the spot size (less than 5%) during scanning. Furthermore, the mirror has been implemented in a high optical throughput micro-optical bench, according to DRIE microfabrication, which enables 200 μm -deep etching of SOI substrates with sidewall verticality better than $90 \pm 0.1^\circ$.

REFERENCES

- [1] Y. M. Sabry, D. Khalil, B. Saadany, and T. Bourouina, "Inclination-independent transformation of light beams using high-throughput uniquely-curved micromirrors," in *Proc. IEEE 27th Int. Conf. Micro Electro Mechanical Syst.*, 2014, pp. 1185–1188.
- [2] H. Cai, X. M. Zhang, C. Lu, and A. Q. Liu, "MEMS variable optical attenuator with linear attenuation using normal fibers," in *Proc. Dig. Tech. Papers Transducers Conf.*, pp. 1171–1174.
- [3] X. M. Zhang *et al.*, "Retro-reflection VOA using parabolic mirror for low insertion loss and linear attenuation relationship," in *Proc. 20th Int. Conf. Micro Electro Mech. Syst.*, 2007, pp. 727–730.
- [4] J. F. Tao *et al.*, "Ultra-high coupling efficiency of MEMS tunable laser via 3-dimensional micro-optical coupling system," in *Proc. IEEE 24th Int. Conf. Micro Electro Mech. Syst.*, 2011, pp. 13–16.
- [5] M. Malak *et al.*, "Stable, high-Q Fabry-Perot resonators with long cavity based on curved, all-silicon, high reflectance mirrors," in *Proc. IEEE 24th Int. Conf. Micro Electro Mech. Syst.*, 2011, pp. 720–723.
- [6] Y. M. Sabry, D. Khalil, B. Saadany, and T. Bourouina, "Integrated wide-angle scanner based on translating a curved mirror of acylindrical shape," *Opt. Exp.*, vol. 21, pp. 13906–13916, 2013.
- [7] Y. M. Sabry, B. Saadany, D. Khalil, and T. Bourouina, "Silicon micromirrors with three-dimensional curvature enabling lens-less efficient coupling of free-space light," *Light Sci. Appl.*, vol. 2, p. e94, 2013.
- [8] Y. M. Sabry, D. Khalil, B. Saadany, and T. Bourouina, "Multi-step etching of three-dimensional sub-millimetre curved silicon microstructures with in-plane principal axis," *Microelectron. Eng.*, vol. 114, pp. 78–84, 2014.
- [9] Z. Moktadir *et al.*, "Etching techniques for realizing optical micro-cavity atom traps on silicon," *J. Micromech. Microeng.*, vol. 14, no. 9, pp. S82–S85, 2004.
- [10] N. Kanbara, S.-I. Tezuka, and T. Watanabe, "MEMS tunable VCSEL with concave mirror using the selective polishing method," in *Proc. IEEE Opt. Micro Electro Mech. Syst.*, 2006, pp. 9–10.
- [11] Y. Ow, M. B. H. Breese, and S. Azimi, "Fabrication of concave silicon micro-mirrors," *Opt. Exp.*, vol. 18, no. 14, pp. 14511–14518, 2010.
- [12] K. Yu, D. Lee, U. Krishnamoorthy, N. Park, and O. Solgaard, "Micromachined fourier transform spectrometer on silicon optical bench platform," *Sens. Actuators A, Phys.*, vol. 130–131, pp. 523–530, 2006.
- [13] C. P. B. Siu, H. Zeng, and M. Chiao, "Magnetically actuated MEMS microlens scanner for in vivo medical imaging," *Opt. Exp.*, vol. 15, no. 18, pp. 11154–11166, 2007.
- [14] H. C. Park, C. Song, and K. H. Jeong, "Micromachined lens microstages for two-dimensional forward optical scanning," *Opt. Exp.*, vol. 18, no. 15, pp. 16133–16138, 2010.
- [15] J. B. Chou, Y. Kyounsgik, and M. C. Wu, "Electrothermally actuated lens scanner and latching brake for free-space board-to-board optical interconnects," *IEEE/ASME J. Microelectromech. Syst.*, vol. 21, no. 5, pp. 1107–1116, Oct. 2012.
- [16] S. T. S. Holmstrom, U. Baran, and H. Urey, "MEMS laser scanners: A review," *J. Microelectromech. Syst.*, vol. 23, no. 2, pp. 259–275, Apr. 2014.
- [17] R. E. Fischer, B. Tadic-Galeb, P. R. Yoder, and R. Galeb, *Optical System Design*. New York, NY, USA: McGraw-Hill, 2000.
- [18] H. Toshiyoshi, W. Piyawattanametha, C. T. Chan, and M. C. Wu, "Linearization of electrostatically actuated surface micromachined 2D optical scanner," *IEEE/ASME J. Microelectromech. Syst.*, vol. 10, no. 2, pp. 205–214, Jun. 2001.
- [19] K. Fuse, T. Okada, and K. Ebata, "Diffractive/refractive hybrid F-theta lens for laser drilling of multilayer printed circuit boards," in *Proc. LAMP Int. Congr. Laser Adv. Mater. Process.*, 2002, pp. 95–100.
- [20] R. Barrett *et al.*, "X-ray microfocussing combined with microfluidics for on-chip X-ray scattering measurements," *Lab Chip*, vol. 6, no. 4, pp. 494–499, 2006.
- [21] J. Adam, A. Mahjoubfar, E. D. Diebold, B. W. Buckley, and B. Jalali, "Spectrally encoded angular light scattering," *Opt. Exp.*, vol. 21, no. 23, pp. 28960–28967, 2013.
- [22] V. P. Maltsev, "Scanning flow cytometry for individual particle analysis," *Rev. Sci. Instrum.*, vol. 71, no. 1, pp. 243–255, 2000.
- [23] Y. M. Sabry, D. Khalil, and T. Bourouina, "Monolithic silicon-micromachined free-space optical interferometers onchip," *Laser Photon. Rev.*, to be published.
- [24] C. Marxer, P. Griss, and N. F. De Rooij, "A variable optical attenuator based on silicon micromechanics," *IEEE Photon. Technol. Lett.*, vol. 11, no. 2, pp. 233–235, Feb. 1999.
- [25] K. Zandi, J. A. Bélanger, and Y. A. Peter, "Design and demonstration of an in-plane silicon-on-insulator optical MEMS Fabry-Pérot-based accelerometer integrated with channel waveguides," *J. Microelectromech. Syst.*, vol. 21, no. 6, pp. 1464–1470, 2012.
- [26] H. Omran *et al.*, "Deeply-etched optical MEMS tunable filter for swept laser source applications," *IEEE Photon. Technol. Lett.*, vol. 26, no. 1, pp. 37–39, Jan. 2014.
- [27] B. Saadany *et al.*, "Free-space tunable and drop optical filters using vertical bragg mirrors on silicon," *IEEE J. Sel. Topics Quantum Electron.*, vol. 12, no. 6, pp. 1480–1488, Nov./Dec. 2006.
- [28] O. Manzardo *et al.*, "Miniature lamellar grating interferometer based on silicon technology," *Opt. Lett.*, vol. 29, no. 13, pp. 1437–1439, Jul. 2004.
- [29] H. Omran, M. Medhat, B. Mortada, B. Saadany, and D. Khalil, "Fully integrated Mach-Zehnder MEMS interferometer with two complementary output," *IEEE J. Quantum Electron.*, vol. 48, no. 2, pp. 244–251, Feb. 2012.
- [30] Y. Sabry, M. Medhat, B. Saadany, A. Safwat, and D. Khalil, "Optical characterization technique for MEMS comb-drive resonators," in *Proc. IEEE/LEOS Int. Conf. Opt. MEMS Nanophoton.*, Aug. 2009, vol. 127–128, pp. 17–20.
- [31] M. Malak *et al.*, "Cylindrical surfaces enable wavelength-selective extinction and sub-0.2 nm linewidth in 250-gap silicon Fabry-Pérot cavities," *J. Microelectromech. Syst.*, vol. 21, no. 1, pp. 171–180, 2012.
- [32] R. R. Syms and A. Lohmann, "MOEMS tuning element for a Lit-trow external cavity laser," *J. Microelectromech. Syst.*, vol. 12, no. 6, pp. 921–928, Dec. 2003.
- [33] O. Manzardo, Y. Petremand, H. P. Herzig, W. Noell, and N. De Rooij, "Micro-sized Fourier spectrometer," *Diffractive Opt. Micro-Opt.*, vol. 75, pp. 119–121, Jun. 2002.
- [34] K. Yu, D. Lee, U. Krishnamoorthy, N. Park, and O. Solgaard, "Micromachined fourier transform spectrometer on silicon optical bench platform," *Sens. Actuators A, Phys.*, vol. 130–131, pp. 523–530, 2006.
- [35] D. Khalil *et al.*, "Characterization of MEMS FTIR spectrometer," *Proc. SPIE*, vol. 7930, pp. 79300J–79300J, 2011.
- [36] A. E. S. M. El Hady, Y. M. Sabry, M. Yehia, and D. Khalil, "Dual-fiber OCT measurements," *Proc. SPIE*, vol. 8934, pp. 3–5, Feb. 2014.
- [37] H. Omran *et al.*, "MEMS optical tunable filter based on free-standing subwavelength silicon layers," *Proc. SPIE*, vol. 8977, pp. 3–6, Feb. 2014.
- [38] P. Goldsmith, *Quasioptical Systems: Gaussian Beam Quasi-Optical Propagation and Applications*. Hoboken, NJ, USA: Wiley, 1998.
- [39] A. Gray, *Modern Differential Geometry of Curves and Surfaces With Mathematica*, 2nd ed. Boca Raton, FL, USA: CRC Press, 1997.
- [40] J. W. Goodman, *Introduction to Fourier Optics*. Roberts and Company Publishers, Englewood, CO, USA, 2005.
- [41] G. Brooker, *Modern Classical Optics*, vol. 8, London, U.K.: Oxford Univ. Press, 2003.
- [42] H. V. Jansen, M. J. De Boer, S. Unnikrishnan, M. C. Louwerse, and M. C. Elwenspoek, "Black silicon method X: A review on high speed and selective plasma etching of silicon with profile control: an in-depth comparison between Bosch and cryostat DRIE processes as a roadmap to next generation equipment," *J. Micromech. Microeng.*, vol. 19, no. 3, p. 033001, 2009.
- [43] D. Lee, K. Yu, U. Krishnamoorthy, and O. Solgaard, "Vertical mirror fabrication combining KOH etch and DRIE of (110) silicon," *J. Microelectromech. Syst.*, vol. 18, no. 1, pp. 2–17–227, 2009.
- [44] O. Solgaard, *Photonic Microsystems: Micro and Nanotechnology Applied to Optical Devices and Systems*. New York, NY, USA: Springer, 2009.
- [45] Y. Nada *et al.*, "Mechanical displacement multiplier: 250 μm stable travel range MEMS actuator using frictionless simple compliant structures," in *Proc. IEEE Conf. Micro Electro Mech. Syst.*, 2012, pp. 1161–1164.
- [46] M. Medhat, Y. Nada, B. Mortada, and B. Saadany, "Long range travel MEMS actuator," U.S. patent application 12 761 621, 2010.

- [47] Y. M. Sabry, D. Khalil, B. Saadany, and T. Bourouina, "Aspherical optical surfaces and optical scanners," U.S. patent application 13 943 846, 2013.



Yasser M. Sabry was born in 1982. He received the B.Sc. and M.Sc. degrees from Ain Shams University, Cairo, Egypt. He received the Ph.D. degree from ESIEE, Paris-Est University Créteil, France, in 2013. From 2005 to 2009, he was Teaching Assistant at Ain Shams University, worked with the transistor modeling team at Mentor Graphics and was a Consultant at the information technology industry development agency ITIDA, Egypt. Since 2008, he has been with the MEMS division of Si-ware Systems where he is currently a Senior Staff and contributed with the team to the development of the SiMOS technology and the world's smallest MEMS-based FTIR spectrometer.



Diaa Khalil received the Ph.D. degree from INPG France in 1992. He is a Professor in the Faculty of Engineering, Ain Shams University, since 2004. He was the Head of the Optical MEMS group in MEMSCAP from 2000 to 2004. Since 2007, he has been the CTO of the MEMS division at Si-ware Systems. He is an inventor of about ten patents, author of more than 160 publications, and the holder of Egyptian state prize in engineering sciences in 1998.



Bassam Saadany received the B.Sc. and M.Sc. degrees in electrical engineering from Ain Shams University, Cairo, Egypt, and the Ph.D. degree in MEMS and nanostructures from the University of Paris XI, France. He is currently MEMS Division Manager with Si-Ware Systems. His background includes optical MEMS design and process development as well as business and R&D management. Before co-founding Si-Ware systems in 2004, he has been with MEMScap, Mentor Graphics, and Enppi.



Tarik Bourouina received the M.Sc. degree in physics, in 1987, the M.Eng. degree in 1988, and the Ph.D. degree in 1991. He received the *Habilitation à Diriger les Recherches* in 2000 from the Université Paris-Sud Orsay in 2000. In 1988, he started his research dedicated to MEMS, holding several positions at ESIEE Paris, at Université Paris-Sud Orsay, at CNRS, at The University of Tokyo and at Si-Ware Systems Corp. His current research interests include micro-photonics, optofluidics and analytical chemistry on chip. Among his contributions to the scientific community, he initiated a research project which led to the development of the world's smallest MEMS-based FTIR spectrometer; a winner product of the Prism Award for Photonics Innovation in 2014. Since 2013, he has been the Editorial Board of *Light: Science and Applications*, Nature Publishing Group. He is currently a Full Professor and the Dean for Research at ESIEE Paris, Université Paris-Est.